Materials Transactions, Vol. 48, No. 1 (2007) pp. 74 to 79

EXPRESS REGULAR ARTICLE

Preparation of Fe–Pt–Si Amorphous Ribbons and Their Coercivity after Crystallization

Tokujiro Yamamoto*[1], Akihiro Omori*[2], Akihiro Makino and Akihisa Inoue

Advanced Research Center of Metallic Glasses, Institute for Materials Research, Tohoku University, Sendai 980-8577, Japan

$Fe_xPt_ySi_z$ ($x = 60$–90, $y = 10$–70, $z = 10$–40) ribbons were prepared using a melt-spinning technique. Fully amorphous ribbons were obtained for alloys containing approximately 20–30 at%Si. Crystallization of the amorphous ribbons yielded composite structures of $L1_0$ FePt and Pt–Si intermetallic compounds for $Fe_{45}Pt_{35}Si_{20}$ and $Fe_{47}Pt_{28}Si_{25}$. $Fe_{45}Pt_{35}Si_{20}$ amorphous ribbons were annealed at 700 K for 180 min, producing a grain size of approximately 40 nm in diameter, and a maximum coercivity of 160 kA/m. [doi:10.2320/matertrans.48.74]

(Received August 10, 2006; Accepted November 17, 2006; Published December 25, 2006)

Keywords: *amorphous materials, nanocrystalline materials, magnetic materials, microstructure*

1. Introduction

Hard magnetic materials are promising materials for the reduction of weight in motors and electric devices, and fine grained alloys with large uniaxial magnetocrystalline anisotropy are desirable for the development of such hard magnetic materials. $L1_0$ tetragonal intermetallic phases, such as FePt, CoPt, FePd and MnAl, are suitable candidates for nanocrystalline hard magnetic materials, because the $L1_0$ phases have large uniaxial magnetocrystalline anisotropy. Among those $L1_0$ intermetallic compounds, FePt with equiatomic composition has large uniaxial magnetocrystalline anisotropy, and saturation of magnetization at room temperature.[1)] Moreover, non-equiatomic $L1_0$ FePt alloys exhibit better magnetic properties than the equiatomic alloy, and Fe–38.5Pt alloy has the largest maximum energy product[2)] among the Fe–Pt binary alloys. For the Fe–Pt binary system, only the $L1_0$ FePt phase has good hard magnetic properties, unlike the other two low temperature equilibrium $L1_2$ phases, Fe_3Pt and $FePt_3$. When the ordered tetragonal $L1_0$ FePt phase is heated, it loses its ferromagneticity at temperatures higher than the Curie temperature, which is approximately 750 K for Fe–50Pt alloys. $L1_0$ FePt then transforms to the fcc (γ-Fe,Pt) phase with further heating.

To obtain nanocrystalline $L1_0$ FePt, two approaches are principally proposed; one is direct synthesis by rapid quenching of molten alloys with Zr and B, and the other is by the crystallization of amorphous alloys.[3,4)] Recently, it was reported that Fe–Pt–B amorphous ribbons were successfully obtained by melt-spinning and that high saturation and residual magnetic flux density (B_s and B_r, respectively) can be achieved by nanocrystallization of the amorphous melt-spun ribbons.[5–7)] The phases found in the ternary Fe–Pt–B as-spun ribbons are summarized in Fig. 1.[3–6,8–13)] In Fig. 1, the composition region for formation of an amorphous phase by rapid quenching is colored gray. It is well-known that $Fe_{80}B_{20}$ alloys form a fully amorphous phase. The composition region where the Fe–Pt–B alloys form an amorphous phase extends towards $Fe_{40}Pt_{20}B_{40}$ from $Fe_{80}B_{20}$. By substitution of Pt for Fe in $Fe_{80}B_{20}$, the amorphous-forming ability of the alloys becomes low, and it seems difficult to obtain an amorphous phase for near equiatomic Fe–Pt alloys with a B content higher than 20 at%, as determined from Fig. 1. As a consequence, it is difficult to find new Fe–Pt–B alloys with excellent magnetic properties, because the amount of $L1_0$ FePt, which is the best hard magnetic compound in the binary alloy system, decreases as the B content in the alloys increases.

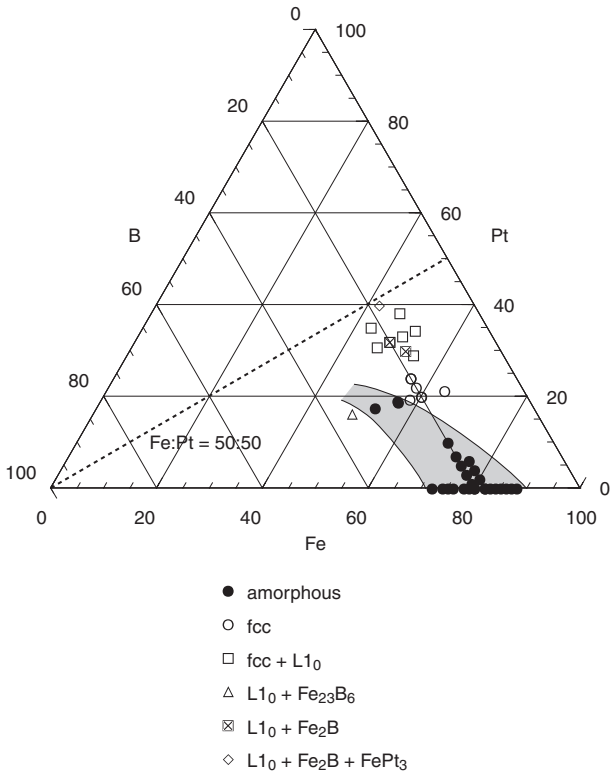

Fig. 1 Phases in Fe–Pt–B as-spun ribbons. The gray region indicates amorphous-forming alloy compositions.

In the present study, the effects of Fe addition to Pt–Si

*[1]Corresponding author, E-mail: toku@imr.tohoku.ac.jp
*[2]Graduate Student, Tohoku University

binary alloys, which typically form an amorphous phase,[14] on the amorphous-forming composition region and the magnetic properties of crystallized Fe–Pt–Si amorphous ribbons were investigated.

2. Experimental Procedures

Ingots with a nominal composition of $Fe_xPt_ySi_z$ ($x = 60$–90, $y = 10$–70, $z = 10$–40) were prepared by arc-melting in an Ar atmosphere. The ingots were rapidly quenched using a melt-spinning technique with a 180 mm diameter Cu roll rotating at 4000 rpm, which resulted in ribbons with a cross section of approximately 1 mm × 10 μm. The crystallization temperature of the as-spun ribbons was measured by differential scanning calorimetry (DSC) at a heating rate of 0.67 K/s. X-ray diffraction (XRD) with a Cu rotating anode, and transmission electron microscopy (TEM) were used for microstructural characterization at room temperature. The as-spun ribbons were crystallized at 750 K and 700 K in an Ar atmosphere within a sealed silica tube. The magnetic properties of the crystallized ribbons were examined using a vibrating sample magnetometer (VSM) at room temperature under a magnetic field applied to the ribbons along their rolling direction.

3. Results

3.1 Phases in Fe–Pt–Si as-spun ribbons

The phases composing all of the as-spun ribbons prepared in this study were identified by XRD. Alloy compositions, for which a fully amorphous phase was obtained, are summarized in Fig. 2. Fully amorphous ribbons are obtained when the Si content is more than 20 at% and less than 40 at%, while all the ribbons contained crystalline phases when the Si content was less than 10 at% and greater than 40 at%. For the as-spun ribbons containing 20 at%Si, nanocrystalline phases tend to precipitate when the Pt content is more than 45 at%, and Fe_3Si silicide is also formed in ribbons with less than 20 at%Pt. Fe_5Si_3, FeSi and other silicides seem to be preferably precipitated in ribbons with 40 at%Si; however, it was difficult to identify these phases. $Fe_{50}Pt_{40}Si_{10}$ as-spun ribbons are composed of almost a single $L1_0$ FePt phase. The composition region where the alloys form a fully amorphous phase is colored gray in Fig. 2. The region is located on the dashed line representing the alloy compositions that contain the same amount of Fe and Pt, and it broadly extends to both $Pt_{80}Si_{20}$ and the opposite Fe–Si binary side along the line representing the $Fe_{100-x}Pt_xSi_{20}$ alloys. The amorphous-forming region of the Fe–Pt–Si ternary system is wider than that of the Fe–Pt–B system, and is closer to the $L1_0$ FePt composition.

3.2 Magnetic properties of crystallized ribbons

In the Fe–Pt binary alloy system, the $L1_0$ FePt phase has the most superior hard magnetic properties. Hard magnetic properties are degraded by adding other elements as the content of Fe in the alloy decreases. Therefore, among the many alloys that form a fully amorphous phase, $Fe_{45}Pt_{35}Si_{20}$ and $Fe_{47}Pt_{28}Si_{25}$ were studied in detail in the present work, because a large amount of $L1_0$ precipitates in those

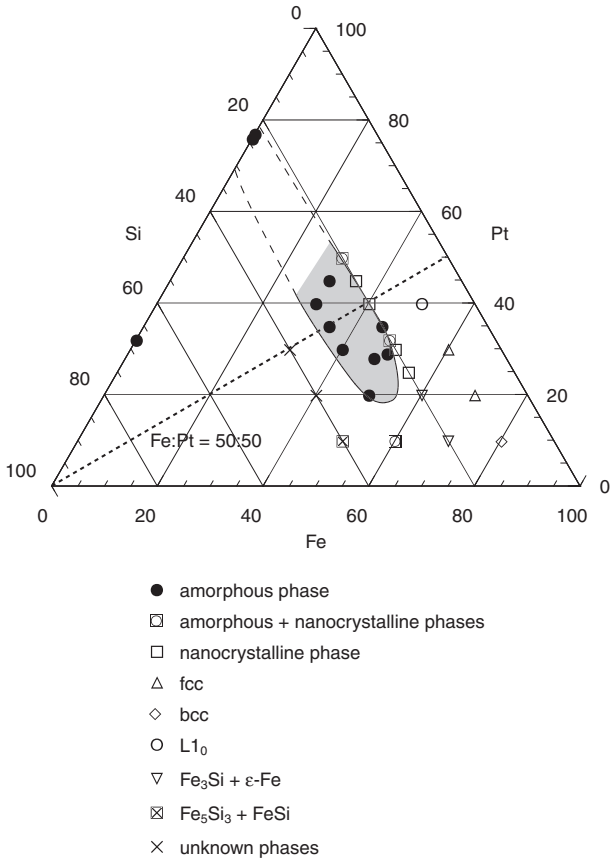

Fig. 2 Phases in Fe–Pt–Si as-spun ribbons. The gray region indicates amorphous-forming alloy compositions. The dashed line represents alloy compositions containing the same amount of Fe and Pt.

amorphous alloys by heat treatment. The composition of $Fe_{45}Pt_{35}Si_{20}$ is the closest to $Fe_{50}Pt_{50}$ among those alloys that form a fully amorphous phase. $Fe_{47}Pt_{28}Si_{25}$ was also studied in order to reveal the effect of microstructure on the magnetic properties of heat-treated Fe–Pt–Si alloys, because $Fe_{47}Pt_{28}Si_{25}$ is also close to $Fe_{50}Pt_{50}$ and because it is expected to exhibit more obvious differences in magnetic properties and microstructure than $Fe_{49}Pt_{29}Si_{22}$ when compared to $Fe_{45}Pt_{35}Si_{20}$.

Figure 3 shows the DSC trace of a $Fe_{45}Pt_{35}Si_{20}$ as-spun ribbon. Any glass transitions could not be detected in the DSC measurement. The crystallization temperature of the ribbon was 679 K. $Fe_{45}Pt_{35}Si_{20}$ and $Fe_{47}Pt_{28}Si_{25}$ as-spun ribbons were heat-treated at 750 K and 700 K, and this was followed by VSM measurements to study the magnetic properties. Figure 4 shows the coercivity of $Fe_{45}Pt_{35}Si_{20}$ and $Fe_{47}Pt_{28}Si_{25}$ crystallized ribbons as a function of heat treatment time at 750 K. The coercivity of crystallized $Fe_{45}Pt_{35}Si_{20}$ ribbons was higher than that of $Fe_{47}Pt_{28}Si_{25}$ for all heat treatment times. With the increase in the heat treatment time, the coercivity of $Fe_{47}Pt_{28}Si_{25}$ ribbons decreased monotonically. The coercivity of $Fe_{45}Pt_{35}Si_{20}$ ribbons also decreased with increasing heat treatment time, although a maximum coercivity of 90 kA/m was obtained when the ribbons were heat-treated for only 30 min. Figure 5 and Figure 6 depict XRD patterns of the heat-treated $Fe_{45}Pt_{35}Si_{20}$ and $Fe_{47}Pt_{28}Si_{25}$ ribbons. Both ribbons crystallized into $L1_0$ FePt, PtSi and Pt_6Si_5 within only 10 min, as no

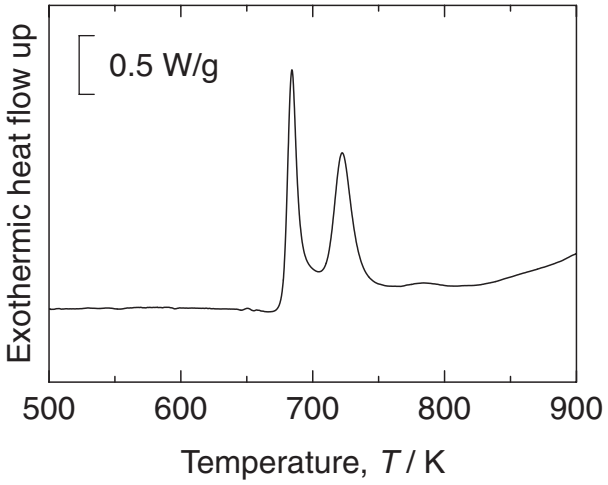

Fig. 3 DSC trace of as-spun $Fe_{45}Pt_{35}Si_{20}$ amorphous ribbons.

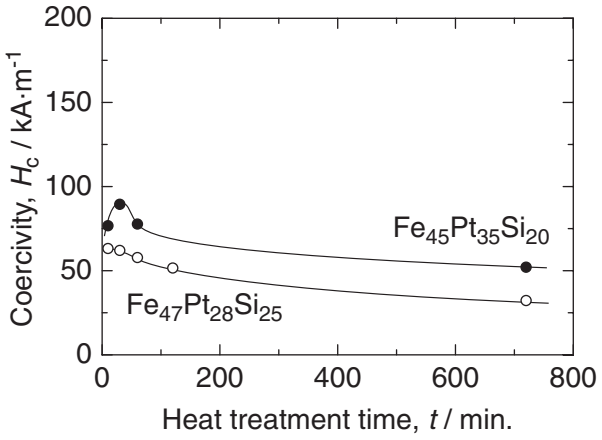

Fig. 4 Coercivity of $Fe_{45}Pt_{35}Si_{20}$ (closed circle) and $Fe_{45}Pt_{35}Si_{20}$ (open circle) ribbons heat-treated at 750 K, as a function of heat treatment time.

amorphous halo was observed in the background of the XRD patterns of those ribbons heat-treated for 10 min. However, the diffraction peaks of $Fe_{45}Pt_{35}Si_{20}$ ribbons heat-treated for 10 min were slightly broader than those for ribbons heat-treated for longer time. It is considered that the $Fe_{45}Pt_{35}Si_{20}$ as-spun ribbons were quickly crystallized within 10 min of heat treatment at 750 K, but some small crystalline grains still remained in the ribbons without grain growth. With increase in the heat treatment time, all the crystal grains became sufficiently large, so that the coercivity of the $Fe_{45}Pt_{35}Si_{20}$ heat-treated ribbons reached a maximum. On the contrary, the $Fe_{47}Pt_{28}Si_{25}$ ribbons were completely crystallized and sufficient crystal grain growth occurred within 10 min, because even slight changes were not found in the XRD patterns of the $Fe_{47}Pt_{28}Si_{25}$ ribbons. Consequently, the coercivity of the $Fe_{47}Pt_{28}Si_{25}$ heat-treated ribbons decreased monotonically with increasing heat treatment time. Because both $Fe_{45}Pt_{35}Si_{20}$ and $Fe_{47}Pt_{28}Si_{25}$ ribbons are crystallized from an amorphous state, the relative intensity of the diffraction peaks of the $L1_0$ FePt phase is generally proportional to the volume fraction of $L1_0$ FePt phase in the crystallized ribbons. It is clear that the intensity of the

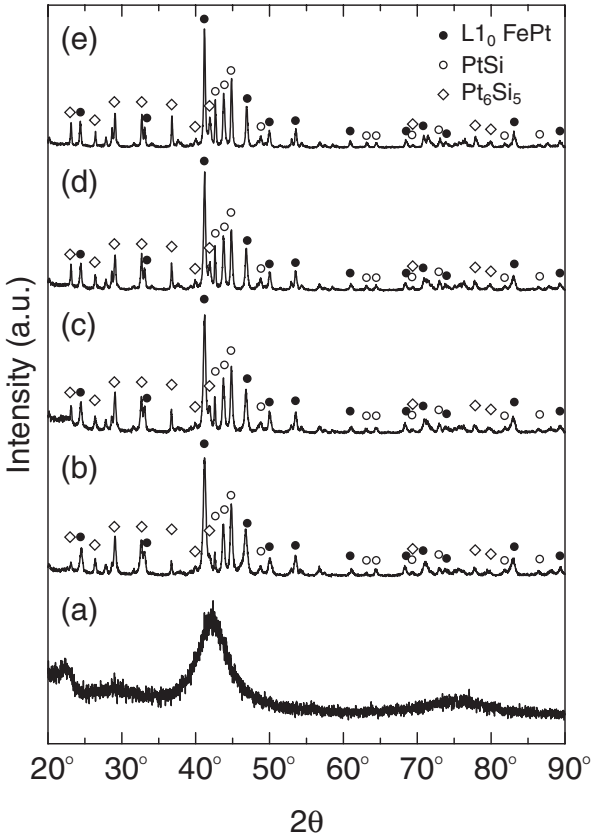

Fig. 5 XRD patterns of $Fe_{45}Pt_{35}Si_{20}$ ribbons heat-treated at 750 K for (a) 0 min, (b) 10 min, (c) 30 min, (d) 60 min, and (e) 720 min.

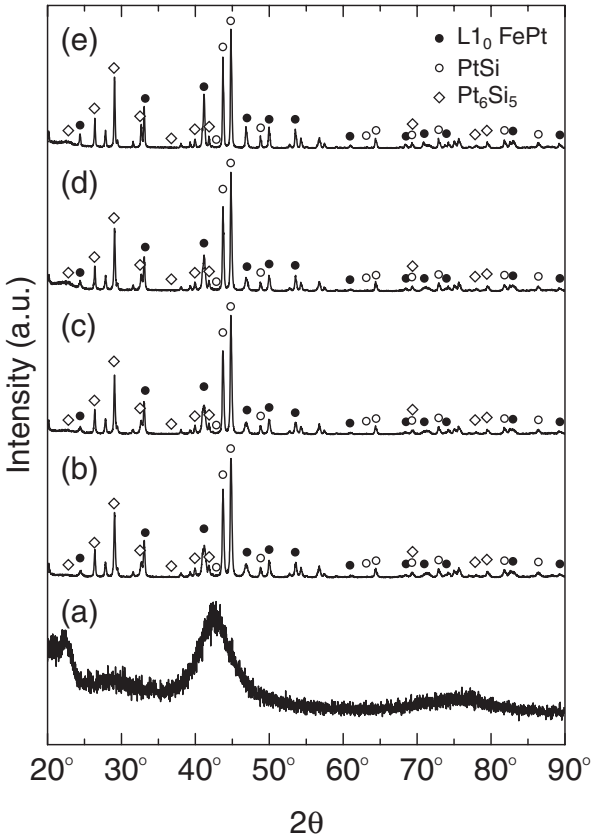

Fig. 6 XRD patterns of $Fe_{47}Pt_{28}Si_{25}$ ribbons heat-treated at 750 K for (a) 0 min, (b) 10 min, (c) 30 min, (d) 60 min, and (e) 720 min.

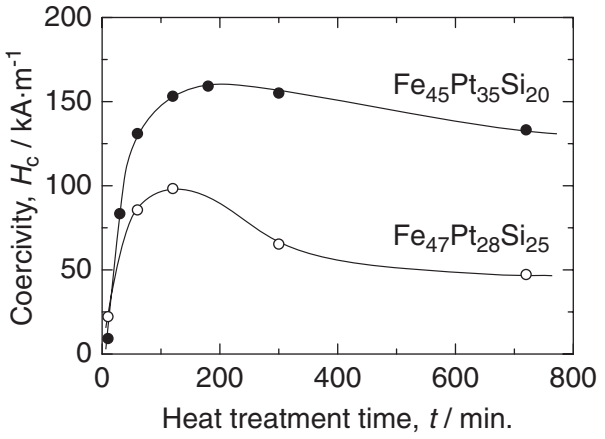

Fig. 7 Coercivity of $Fe_{45}Pt_{35}Si_{20}$ (closed circle) and $Fe_{45}Pt_{35}Si_{20}$ (open circle) ribbons heat-treated at 700 K, as a function of heat treatment time.

diffraction peaks of $L1_0$ FePt, which is the only ferromagnetic phase in the ribbons, is larger for heat-treated $Fe_{45}Pt_{35}Si_{20}$ than for $Fe_{47}Pt_{28}Si_{25}$, in accordance with the coercivity of the heat-treated ribbons. However, the amount of $L1_0$ FePt in heat-treated Fe–Pt–Si ribbons seems to be less than that in heat-treated Fe–Pt–B ribbons.[3,4,6,13)]

Because Fe–Pt–Si ternary amorphous ribbons are crystallized so quickly at 750 K, both $Fe_{45}Pt_{35}Si_{20}$ and $Fe_{47}Pt_{28}Si_{25}$ amorphous ribbons were subjected to heat treatment at a lower temperature of 700 K, in order to decrease the crystallization rate. The coercivity of the heat-treated ribbons was then measured as a function of heat treatment time, as shown in Fig. 7. $Fe_{45}Pt_{35}Si_{20}$ ribbons reached a maximum coercivity of 160 kA/m after heat treatment for 3 h, and a maximum coercivity of 100 kA/m was obtained for $Fe_{47}Pt_{28}Si_{25}$ ribbons after heat-treatment for 2 h. XRD measurements and TEM observations were carried out for $Fe_{45}Pt_{35}Si_{20}$ ribbons, whose coercivity was higher than that of $Fe_{47}Pt_{28}Si_{25}$ ribbons for all heat treatment times. The XRD patterns of pulverized $Fe_{45}Pt_{35}Si_{20}$ ribbons were measured to investigate the volume fraction of $L1_0$ FePt phase in the ribbons as a function of heat treatment time and are shown in Fig. 8. The relative intensity of the diffraction peaks for $L1_0$ FePt increased as the heat treatment time was increased, compared with PtSi and Pt_6Si_5, while the peak widths for $L1_0$ FePt decreased. On the other hand, the 2θ angles of the 200 and 002 peaks for $L1_0$ FePt did not change with increasing heat treatment time. These results imply that the $L1_0$ FePt crystal grain size increased without change in the crystalline/amorphous ratio of $L1_0$ FePt. Figure 9 shows the TEM microstructure of $Fe_{45}Pt_{35}Si_{20}$ ribbons that were heat-treated for 3 h, and exhibited maximum coercivity. The dark field image, shown in Fig. 9(b), was taken by selecting several diffraction spots, including those of $L1_0$ FePt, because it was difficult to select only the diffraction spots of $L1_0$ FePt using the objective aperture of the TEM. However, it was clearly determined that the crystal grain size of the $L1_0$ FePt phase in $Fe_{45}Pt_{35}Si_{20}$ heat-treated ribbons with the maximum coercivity was approximately 40 nm. The grain size is almost the same as that of the $L1_0$ FePt phase in Fe–Pt–B ternary ribbons with hard magneticity.[5,6)]

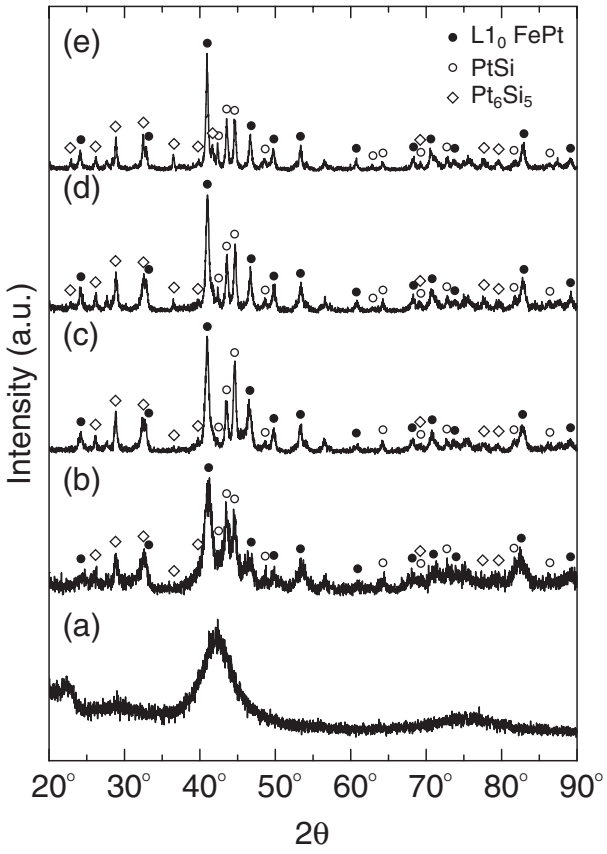

Fig. 8 XRD patterns of pulverized $Fe_{45}Pt_{35}Si_{20}$ ribbons heat-treated at 700 K for (a) 0 min, (b) 10 min, (c) 60 min, (d) 180 min, and (e) 720 min.

4. Discussion

The enthalpy of mixing, ΔH^{mix}, and the atomic size difference, Δr, of Fe, Pt, Si and B are tabulated in Table 1.[15)] The ΔH^{mix} and Δr for Fe and Pt are -13 kJ/mol and 12.1%, respectively. When the Fe–Pt–Si system is compared with Fe–Pt–B, the absolute value of ΔH^{mix} for Fe–Si and Pt–Si is much larger than that for Fe–B and Pt–B, although the Δr for Si and other constituent elements is much smaller than that for B. In Fe–Pt-based ternary alloy systems, it appears that the effect of ΔH^{mix} is more significant than that of Δr for the formation of amorphous alloys.

When a $Fe_{50}Pt_{50}$ alloy is rapidly quenched, fcc (γ-Fe,Pt) is obtained. In this study, almost single phase $L1_0$ FePt was directly obtained by rapid quenching from molten $Fe_{50}Pt_{40}Si_{10}$ alloys, and melt-spun ribbons consisted of an almost fully amorphous phase when more than 20 at%Si was added to $Fe_{50}Pt_{50}$. Therefore, it is considered that the formation of a stable phase during rapid quenching depends on the Si content of the alloy. Figure 10 schematically illustrates the experimentally determined Gibbs free energies for liquid (G_L), fcc (γ-Fe,Pt) (G_γ), $L1_0$ (G_{L1_0}) and silicide phases (G_C) at slightly higher temperature than the crystallization temperature of the molten alloy, as a function of Si content. Alloys with low Si content, c_1, such as $Fe_{50}Pt_{50}$, transform to fcc (γ-Fe,Pt) during rapid quenching. When the Si content is c_2, $Fe_{50}Pt_{40}Si_{10}$, the liquid transforms to $L1_0$ rather than to (γ-Fe,Pt), because G_{L1_0} has the lowest Gibbs

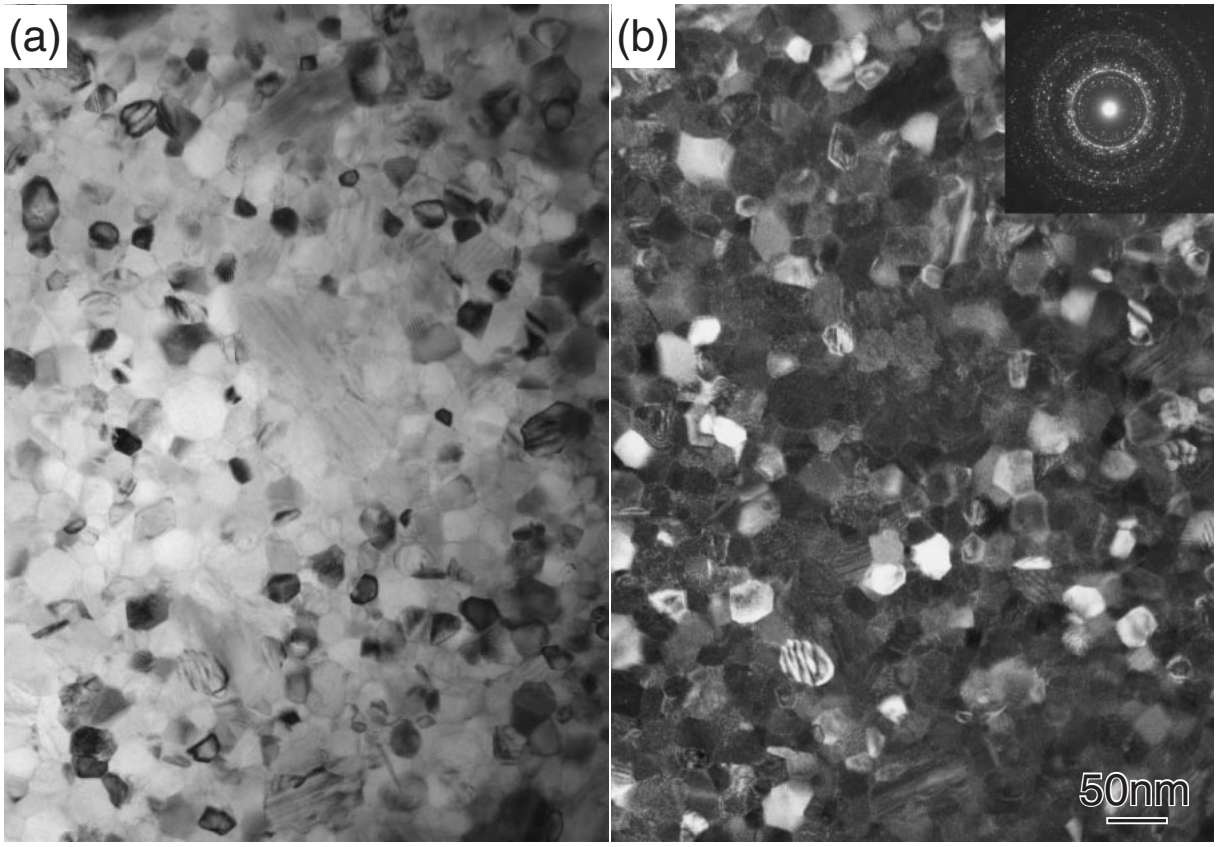

Fig. 9 TEM (a) bright field and (b) dark field images of $Fe_{45}Pt_{35}Si_{20}$ ribbons heat-treated at 700 K for 3 h.

Table 1 Enthalpy of mixing ΔH^{mix} (kJ/mol) and atomic size difference Δr (%) for Fe, Pt, Si and B.[15)]

	Fe		Pt	
	ΔH^{mix}	Δr	ΔH^{mix}	Δr
Si	−18	6.0	−36	18.8
B	−11	37.8	−13	54.5

free energy. For alloys with high Si content, c_3, long range diffusion is required to reach an equilibrium state consisting of the $L1_0$ phase and silicides, as indicated by the dash-dotted line in Fig. 10. Therefore, an amorphous phase is obtained by quenching. Alloys with greater Si content, c_4, transform to silicides. As a consequence, Si addition decreases G_{L1_0}, and disturbs the diffusion of atoms, and stabilizes the liquid phase in the Fe–Pt–Si ternary alloy system.

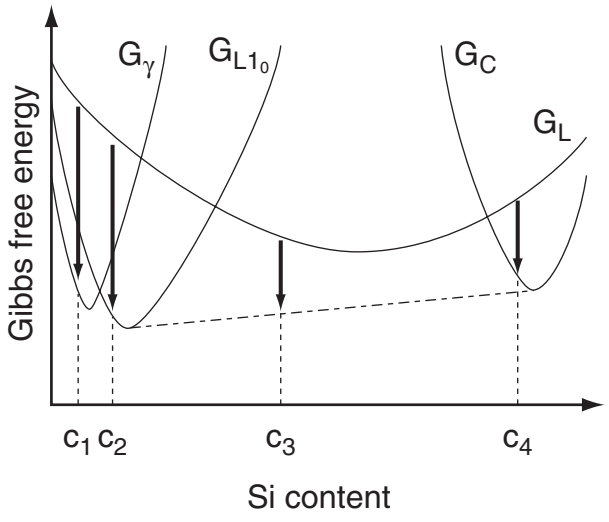

Fig. 10 Schematic diagram of Gibbs free energies for liquid (G_L), fcc (γ-Fe,Pt) (G_γ), $L1_0$ FePt (G_{L1_0}) and Fe–Si intermetallic compound (G_C), as a function of Si content.

5. Conclusions

Fe–Pt–Si ternary amorphous alloy ribbons were prepared using a melt-spinning technique. Figure 2 indicates the alloy composition region for the formation of an amorphous phase, which is located on the dashed line representing the alloy compositions containing the same amounts of Fe and Pt, and broadly extends to both $Pt_{80}Si_{20}$ and the opposite Fe–Si binary side along the line representing the $Fe_{100-x}Pt_xSi_{20}$ alloys. The amorphous-forming region of the Fe–Pt–Si ternary system found in the present study is wider than that of the Fe–Pt–B system, and is closer to a $L1_0$ FePt composition. The $Fe_{45}Pt_{35}Si_{20}$ ribbons crystallized as $L1_0$, PtSi and Pt_6Si_5 phases and exhibited a maximum coercivity of approximately 160 kA/m after heat treatment at 700 K for 3 h. Heat-treated $Fe_{45}Pt_{35}Si_{20}$ ribbons showed a crystal grain size of 40 nm with a maximum coercivity of 160 kA/m. However, the amount of $L1_0$ FePt phase in heat-treated $Fe_{45}Pt_{35}Si_{20}$ was less than that in the heat-treated Fe–Pt–B alloys.

Acknowledgments

The authors would like to thank Mr. Kenichiro Sasamori and Mr. Yoshihiro Murakami of the Advanced Research Center of Metallic Glasses, Institute for Materials Research (IMR), Tohoku University (TU) for assisting the authors with specimen preparation and quantitative analyses, respectively. Part of this work was carried out at the COE Laboratory, IMR, TU. Some experiments in this work were performed using equipment supported by Research and Development Project on Advanced Metallic Glasses, Inorganic Materials and Joining Technology, IMR, TU. This work was supported by a Grant-in-Aid for Young Scientists (B) 17760556 and a Grant-in-Aid for Scientific Research on Priority Areas "Materials Science of Bulk Metallic Glasses" from the Ministry of Education, Culture, Sports, Science and Technology.

REFERENCES

1) O. A. Ivanov, L. V. Solina, V. A. Demshina and L. M. Magat: Phys. Met. Metallogr. **35** (1973) 81.
2) K. Watanabe and H. Masumoto: Trans. JIM **24** (1983) 627.
3) A. Makino and T. Bitoh: J. Appl. Phys. **95** (2004) 7498.
4) A. Makino, T. Bitoh and A. Inoue: Mater. Trans. **45** (2004) 2909.
5) W. Zhang, D. V. Louzguine and A. Inoue: Appl. Phys. Lett. **85** (2004) 4998.
6) A. Inoue, W. Zhang, T. Tsurui and D. V. Louzguine: Mater. Trans. **46** (2005) 891.
7) D. V. Louzguine, W. Zhang and A. Inoue: J. Alloys Comp. **402** (2005) 78.
8) R. Hasegawa, R. C. O'Handley, L. E. Tanner, R. Ray and S. Kavesh: Appl. Phys. Lett. **29** (1976) 219.
9) R. Hasegawa and R. Ray: J. Appl. Phys. **49** (1978) 4174.
10) J. L. Walter: Mater. Sci. Eng. **50** (1981) 137.
11) K. Inomata, T. Sawa and S. Hashimoto: J. Appl. Phys. **64** (1988) 2537.
12) E. Nowakowska, P. Duda, J. Grabski, E. Gradys, R. Kupczak, J. Oleniacz and W. Zych: Phys. Stat. Sol. (a) **185** (2001) 277.
13) W. Zhang, K. Yubuta, P. Sharma and A. Inoue: J. Appl. Phys. **99** (2006) 08E914.
14) R. C. Crewdson: Calif. Tech. Rep. **CALT-221-20** (1966) 21.
15) A. Takeuchi and A. Inoue: Mater. Trans. **46** (2005) 2817.